Analysis of suprathermal tails using hourly-averaged proton velocity distributions at 1 AU

G. Gloeckler, L. A. Fisk, G. M. Mason, E. C. Roelof, and E. C. Stone

Citation: AIP Conference Proceedings **1436**, 136 (2012); doi: 10.1063/1.4723601
View online: http://dx.doi.org/10.1063/1.4723601
View Table of Contents: http://scitation.aip.org/content/aip/proceeding/aipcp/1436?ver=pdfcov
Published by the AIP Publishing

Analysis of Suprathermal Tails Using Hourly-averaged Proton Velocity Distributions at 1 AU

G. Gloeckler [a], L. A. Fisk [a], G. M. Mason[b], E. C. Roelof [b] and E. C. Stone [c]

[a]*Department of Atmospheric, Oceanic, and Space Sciences, University of Michigan*
2455 Hayward Street, Ann Arbor, MI 48109-2143, USA
[b]*Applied Physics Laboratory, Johns Hopkins University, Laurel, MD 20723, USA*
[c]*California Institute of Technology, Mail Code 220-47, Pasadena, CA 91125, USA*

Abstract. We obtain hourly values of tail densities and of power law indices, γ, of suprathermal (speeds above 2.48 times the solar wind speed) protons from power law fits to hourly velocity distribution functions in the solar-wind-frame. ACE/SWICS and ULEIS data, which often include very low counting statistics, are used to derive hourly proton phase space densities. We find that during part of the recent deep solar minimum (first 82 days in 2009): *(a)* the spectrum averaged over the entire 82 day period reveals the bulk and the halo solar wind components, interstellar pickup protons (seldom seen at 1 AU), and the common Fisk and Gloeckler (F&G) suprathermal tail (v^{-5} in velocity v with an exponential rollover at some higher speed); *(b)* hourly values of the tail densities range from ~$1 \cdot 10^{-6}$ to ~$3 \cdot 10^{-3}$ cm^{-3} and vary by a factor of ~2-10 over periods of hours as well as in a quasi-periodic manner by factors of 20 to 50 over 4 to 10 days; *(c)* about 95% of the nearly 2000 hourly spectra have complex shapes and that are not power laws; *(d)* about half of the ~5% of the hourly spectra that are monotonically decreasing with increasing speed (e.g. exponentials or Maxwellians, or F&G) are observed at times of high tail densities (>~$5 \cdot 10^{-5}$ cm^{-3}) where the spectra have the common F&G shapes; *(e)* each of the six sharp (few day long), large (tail density > $5 \cdot 10^{-4}$ cm^{-3}) increases observed during this time period is associated with solar wind compression regions; *(f)* the eight shocks recorded locally that were not contained in compression regions did not produce significant increases in the tail densities. We conclude that during times of low solar activity the higher energy portions of locally accelerated suprathermal tail spectra are often obscured by significant contributions from remotely accelerated particles whose spectra below (1-3)$\cdot 10^8$ cm/s are modified (modulated) by propagation from this remote acceleration region. In those instances where strong acceleration occurs locally, the observed tail spectra have the common F&G spectral shapes.

Keywords: Particle acceleration, suprathermal tails.
PACS: 96.50.Pw, 96.50.Qx, 95.50.Ci, 96.50.Ya

INTRODUCTION

Observations of v^{-5} (or -5 power law) suprathermal tails (or tails, hereafter) with exponential rollovers (common spectral shape or F&G spectra, hereafter) on the velocity distributions of solar wind and pickup ions have been well documented [1-6]. In most of these publications long time averages (days to years) were used to obtain sufficient counting statistics, especially during "quiet" times when tail densities were low. In order to characterize the properties of these proton tails and determine their origin, we examine the behavior of suprathermal particles with speeds above the pickup H^+ cutoff, on scales of the correlation length of the solar wind by analyzing one-hour averaged proton spectra.

Physics of the Heliosphere: A 10 Year Retrospective
AIP Conf. Proc. 1436, 136-143 (2012); doi: 10.1063/1.4723601

METHODOLOGY

To obtain hourly velocity distributions we use one of several possible analysis methods to treat data of very low counting statistics [7]. The SWICS instrument [8] on ACE measures the counting rate C_i of protons (and other ions species not discussed here) in each of a sequence of 60 logarithmically spaced energy steps (from 0.49 to 100 keV/charge). This sequence is repeated every 12 minutes as described in detail in [8,9]. For this study we accumulate proton counts in 9 consecutive W (the measured proton speed, V_p, divided by the simultaneously measured solar wind speed, V_{sw}) intervals (called SWICS points) of increasing width ($1.86 < W_1 \leq 2.15 < W_2 \leq 2.48 < W_3 \leq 2.86 < W_4 \leq 3.29 < W_5 \leq 3.94 < W_6 \leq 4.70 < W_7 \leq 5.82 < W_8 \leq 7.47 < W_9 \leq 9.93$). In a one hour accumulation time, and especially during quiet solar wind conditions, the proton counts in a given W_i interval, from which the proton phase space density, F_i, is computed [9], can be extremely low, often consisting of a string of k zeros followed by $n \geq 1$ counts. Assuming Poisson statistics and using maximum likelihood arguments we replace each of the k zeros and the first non-zero count in a given (k+1) string with $n/(k+1)$ and assign to each a statistical error of $n^{1/2}/(k+1)$. We also replace each of the k 'zero' phase space densities, $F_0 = 0$, values and the first non-zero F_n in the corresponding (k+1) string with $F_n/(k+1)$ and assign to each a statistical error of $F_n \bullet n^{1/2}/(k+1)$. Thus, for each hour we obtain an estimate of a 9-point velocity distribution, or phase space density as a function of particle speed in the spacecraft frame of reference.

The transformation of a full 3D solar wind frame velocity distribution to the spacecraft frame can be done precisely using an updated forward model of the SWICS instrument response that requires input of the solar wind flow direction and the ACE spin axis direction. However, to reverse this process would require a lengthy iterative procedure of running the forward model repeatedly, assuming various solar wind frame distributions, until a match to the spacecraft measured spectrum is obtained. Such a procedure is difficult to implement in an automatic fashion. Instead, we use here a fairly good approximate transformation from the spacecraft to the solar wind frame, assuming isotropic solar wind frame distributions and ignoring the small changes in the spin axis pointing direction. With these simplifications, each measured $F(V_p)$ transforms to $F(v_p)$, where the proton speed in the solar wind frame, $v_p = V_p - h(V_p,\gamma_{sc}) \times V_{sw}$, V_p is the measured proton speed, and γ_{sc} is the power law index computed from any two adjacent $F(V_p)$ values. The forward model is applied to power law spectra that are isotropic in the solar wind frame to determine $h(V_p,\gamma_{sc})$.

RESULTS

In order to compare with previous studies of tails [1-6] we show in Fig. 1a the solar wind frame velocity distribution averaged over the entire 82-day time period. The spectrum is extended to proton speeds below W_1 using our standard fine-resolution analysis [9]. Here, the transformation to the solar wind frame was done iteratively using the SWICS forward model. Consistent with previous results, e.g. [3], we find a four-component spectrum consisting of (a) the bulk solar wind [11], (b) the much hotter halo solar wind, visible between ~$1 \bullet 10^7$ and ~$3 \bullet 10^7$ cm/s, (c) interstellar pickup H^+ at ~ $4 \bullet 10^7$ cm/s, and (d) the suprathermal tail above the cutoff speed of pickup H^+. The halo solar wind, so clearly visible, is not simply a κ-function tail extension of the bulk solar wind,

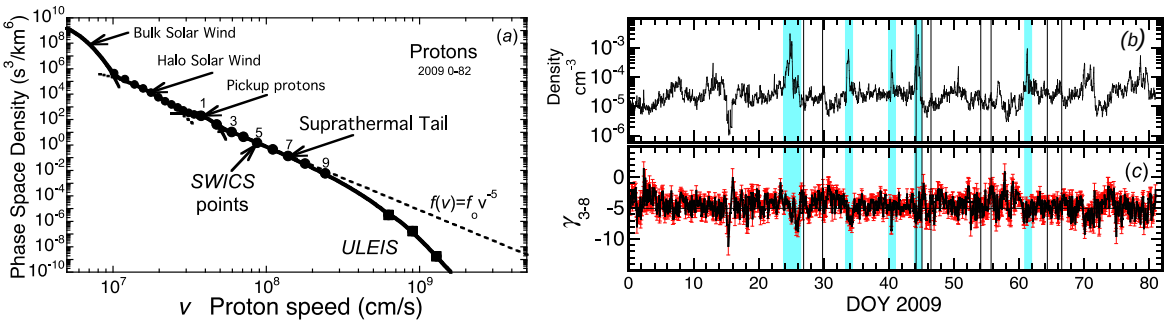

FIGURE 1. *(a)*: Velocity distribution in the solar wind frame, averaged over the first 82 days of 2009, measured with ACE/SWICS and ULEIS [8,10]. Transformation to the solar wind frame assumes isotropic solar wind frame distributions. The four components discussed in the text are clearly distinguishable. The bulk solar wind is represented by a Maxwellian with a speed of 393 km/s, a density of 6.6 cm^{-3} and a thermal speed of 30.2 km/s (from [11]). The densities in units of cm^{-3} and (pressures in units of dyne/cm^2) of the other three components are: 0.0095 ($5.5\bullet10^{-13}$), 0.00014 ($1.4\bullet10^{-13}$), and $3.1\bullet10^{-5}$ ($1.8\bullet10^{-13}$) for the halo solar wind [3] characterized by a κ-function ($\kappa = 6.5$), interstellar pickup H^+ and the suprathermal tail whose shape is a v^{-5} power law with an exponential rollover at e-folding speed of $1.8\bullet10^8$ cm/s. The tail pressure is comparable to the pickup H^+ pressure and ~26% of the sum of halo and pickup H^+ pressures. *(b,c)*: Hourly values of *(b)* tail density, computed from phase space densities using points 2 through 8 labeled in *(a)*, and of *(c)* spectral indices, $\gamma_{3\text{-}8}$. (obtained from weighted power law fits to phase space density points 3-8) with their 1-σ errors, *versus* DOY (day of year) of 2009.

but a separate hot component well represented by a κ-function. During more active times, interstellar pickup protons are either not present or seldom visible at 1 AU, being swamped by the halo solar wind. The fact that we see them here implies that during minimum solar activity, interstellar hydrogen reaches distances well below 1 AU, and that the halo temperature is low enough to barely expose the pickup H^+ peak. The suprathermal tail, visible above $\sim5.5\bullet10^7$ cm/s, is a power law with a gradual exponential rollover that begins at $\sim2\bullet10^8$ cm/s. A weighted least squares fit of an F&G spectrum having the form $f = f_o v^{-\gamma}\exp(-v/v_o)$ to the SWICS data (excluding points 1 and 2 that are mostly pickup protons) and the three lowest energy ACE ULEIS proton points, gives $\gamma = 4.99 \pm 0.01$ and $v_o = (1.704 \pm 0.009) \bullet10^8$ cm/s.

Six large (factor of ~20 to ~100 or more), rapid (hours) increases in the tail density, each lasting a fraction of a day, were observed (one or more in each of five shaded regions of Fig. 1b and, in more detail, in the third from top panel of Fig. 2). The peak of each of the increases coincides with, or immediately follows, a compression region – significant, rapid (hours) increases in solar wind density, usually accompanied by an increase in solar wind bulk speed. These fraction-of-day long tail density increases are most likely instances of local, or close to local, acceleration of tails, associated with local solar wind compression regions. None of the eight shocks (indicated by vertical lines in Figs. 1b, 1c and 2) observed outside the compression regions produced substantial increases in tail densities. The predominance of large σ seen in Figs. 1c and bottom panel of 2 implies that most of the hourly tail spectra are not well characterized by power laws.

In Fig. 3a we show time-averaged velocity distributions in the solar wind frame during (1) the one-hour of maximum observed tail density (0.003 cm^{-3}, filled circles), and (2) during 19 consecutive hours of minimum average tail density (0.000053 cm^{-3}, filled triangles). The maximum density spectrum is well fit using the common (F&G) spectral shape. The best values for $\gamma_{F\&G}$ and the e-folding rollover speed are -4.95 ± 0.05 and $(1.66 \pm 0.40)\bullet10^8$ cm/s respectively, with α, the sharpness of the cutoff held at 1.65. The

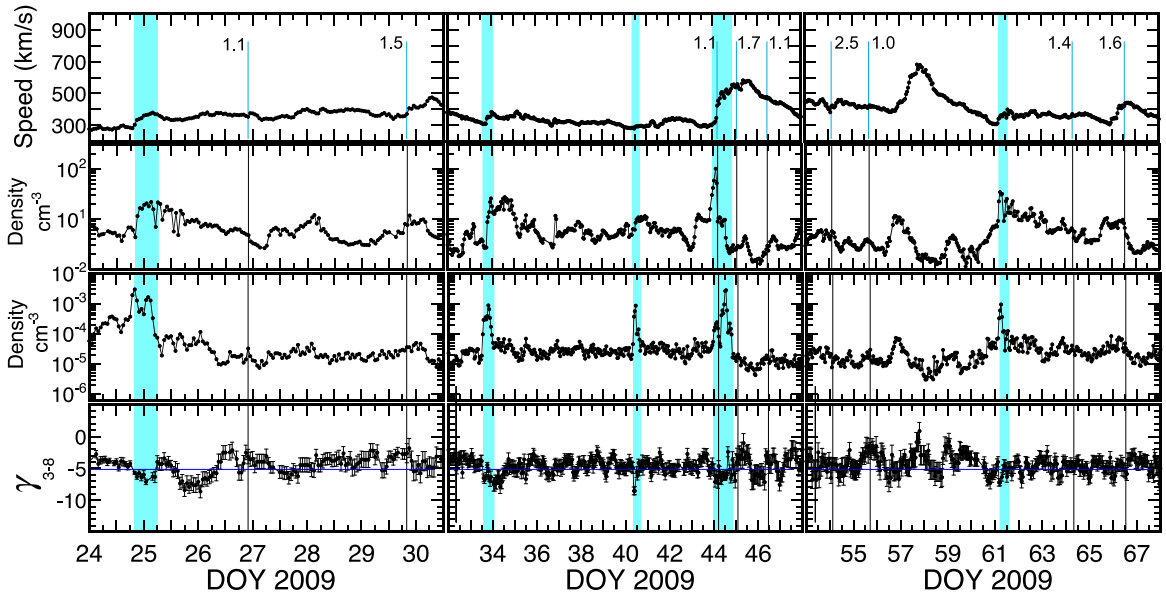

FIGURE 2. *(top to bottom)*: Hourly values *versus* DOY (day of year) of 2009 of solar wind speed, solar wind density, tail density and spectral index, $\gamma_{3\text{-}8}$ during a one-week *(left and right panels)*, and two-week *(center panel)* period. Shaded regions contain one or more local acceleration events (large, rapid increases of the tail densities, each lasting ~4 to ~8 hours). Between these acceleration events, hourly tail densities vary quasi-randomly by factors of ~2 to 10 over periods of one to several hours. Hourly spectral indices $\gamma_{3\text{-}8}$ *(bottom panel)* of power law fits to the 6-point solar wind frame velocity distributions cluster around -5, but also show significant systematic variations on a scale larger than the $\pm$ 1-σ uncertainties (error bars). Typical errors in $\gamma_{3\text{-}8}$ are $\pm$2.5, indicating that power laws poorly represent most of the hourly velocity distributions. The observation times of local shocks and their respective compression ratios [12] are indicated by vertical line and values listed next to these lines.

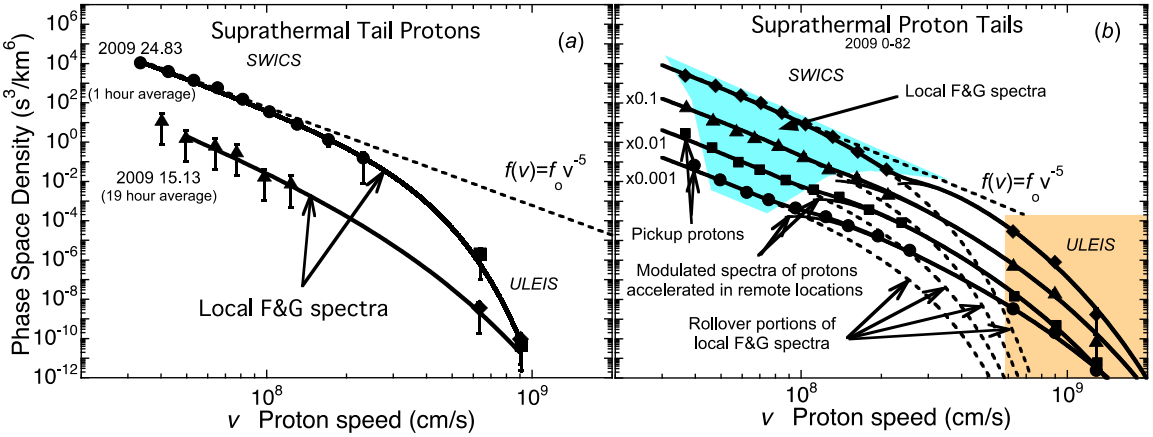

FIGURE 3. Solar wind frame velocity distributions (assumed to be isotropic) *versus* proton speed. *(a)*: one-hour averaged spectrum starting on DOY 24.83 during the highest, and a 19-hour averaged spectrum starting on DOY 15.13 during the lowest observed tail density in the first 82 days of 2009. *(b)*: average of individual 1-hour spectra selected according to tail densities, n_{tail}: $>3\bullet10^{-4}$ cm^{-3} (diamonds), $1\bullet10^{-4} < n_{tail} < 3\bullet10^{-4}$ cm^{-3} (triangles), $3\bullet10^{-5} < n_{tail} < 1\bullet10^{-4}$ cm^{-3} (squares), and $1\bullet10^{-7} < n_{tail} < 3\bullet10^{-5}$ cm^{-3} (circles). Fits of the form $f(v) = f_o v^{-\gamma}\exp(-(v/v_o)^{\alpha})$ to the visible portions of the local spectra (i.e. in speed range contained in the upper shaded region) give γ values of 4.95 $\pm$0.013, 4.95 $\pm$0.043, 5.06 $\pm$0.03 and 5.01 $\pm$0.04 for spectra shown by diamonds, triangles, squares and circles respectively. In each case v_o is fixed at $1.1\bullet10^8$ cm/s, and α, the sharpness of the cutoff, at 1.5.

minimum-density spectrum, excluding the lowest energy (speed) point that has contributions from pickup protons, is also well fit using the F&G spectral shape, with the best value for $\gamma_{F\&G}$ of -5.07 ±0.54, an e-folding rollover speed of (1.58±0.14)•10^8 cm/s with α held at 1.4. Shown in Fig. 3b are averaged velocity distributions using individual hourly spectra selected within four specified ranges of tail densities. None of the four spectra shown have a simple F&G shape. The spectra are complex or compound, being a combination of F&G spectra at low speeds, and, at higher speeds modulated spectra of particles propagating from remote acceleration sites. With decreasing tail densities, the low-energy locally accelerated spectra become less obvious, being visible only over progressively smaller speed ranges (see upper shaded region in Fig. 3b). The lowest and higher energy portions of the F&G spectra are progressively more obscured by pickup protons and modulated spectra of remotely accelerated protons, respectively.

Schwadron et al. [13] have suggested that v^{-5} velocity distributions can be created simply by averaging many individual exponential or Maxwellian spectra, with spectral parameters changing according to Poisson statistics over appropriately short (e.g. one hour) time intervals. In order to test this hypothesis, we sorted our measured hourly spectra according to one of several selection criteria to determine if an individual hourly spectrum had an F&G, an exponential or a Maxwellian shape in the SWICS energy range. The least stringent selection rule required that the phase space density, F_k, associated with each SWICS point (k = 1 through 9) was greater than that of the following point (i.e. $F_k/F_{k-1} \leq 1$). This resulted in 383 out of a total of 1944 (~20%) satisfying this criterion (type I spectra) with the other 80% having complex spectral shapes with at least one $F_k/F_{k-1} > 1$ (type II spectra). The most stringent selection rule required that the spectral index γ_k, determined from weighted power law fits to three consecutive SWICS points, k-1, k and k+1 satisfied the criterion $\gamma_k/\gamma_{k-1} > 1$ (type III spectra). Five (~0.3%) out of 1712 hourly spectra were type III. We also selected spectra using selection criterion of intermediate restrictions (type IV spectra), requiring $\gamma_k/\gamma_{k-1} > 1$ over an energy range that excluded any possible contributions from pickup protons (k = 2 through 9). About 5.4%

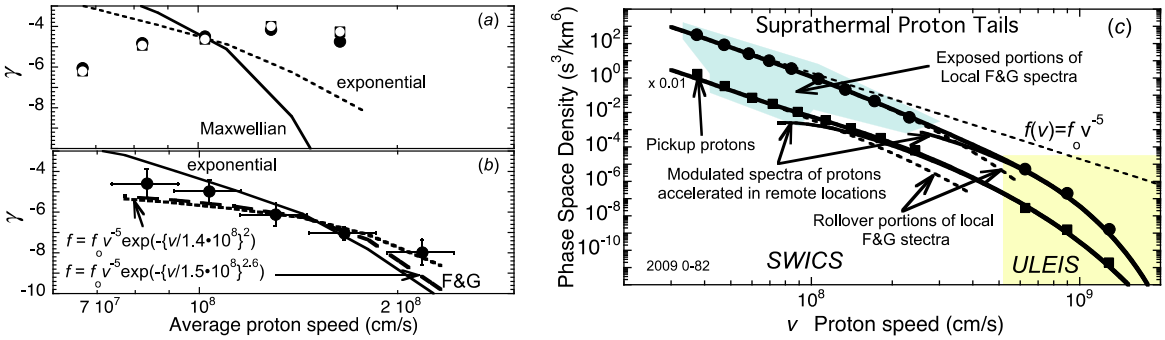

FIGURE 4. *(a)* and *(b)*: Variations of $\gamma(v)$ values with average proton speed v. $\gamma(v)$ is the mean (filled circles) and median (unfilled squares) of selected (see text for selection rules) individual hourly indices obtained from weighted power law fits to three consecutive SWICS points with the center point corresponding to the speed of that point. Values of $\gamma(v)$ of type V spectra are shown in panel *(a)* and those of type III spectra in *(b)*. Error bars indicate the standard errors of v and $\gamma(v)$ respectively. Also shown as curves in panel *(a)* are γ values computed for exponentials (dashed curve), and Maxwellian (solid curve) spectral shapes and, in panel *(b)* for exponentials (solid curve) as well as two F&G spectra with different rollover parameters (dashed and dotted curves). Panel *(c)*: Solar-wind-frame velocity distributions obtained from averages of individual hourly spectra of type I (filled circles) or type II (filled squares)..

(104 out of 1925) hourly spectra were type IV, while the other 94.6% were type V spectra. It is obvious from Fig. 4a that the majority (94.6%) of all individual hourly spectra (type V) are complex, being neither exponential, nor Maxwellian, nor simple power laws, nor F&G spectra. The 5 hourly spectra that satisfied the most stringent selection criterion (type III) were closest to F&G shapes and only marginally exponentials (Fig 4b). The average velocity distribution (filled circles in Fig. 4c) of the 383 individual type I hourly spectra has the F&G shape over the entire SWICS range. However, in the higher ULEIS energy range a modulated spectrum from a presumably remote acceleration region obscures the high end of the F&G spectrum. The average spectrum (filled squares in Fig. 4c) of the 1821 type II hourly spectra is a complex spectrum with the F&G spectrum obscured by pickup protons at the lowest SWICS energy and by the modulated spectrum of particles accelerated at a remote site in the upper energy range of SWICS and also in the ULEIS energy range.

SUMMARY, DISCUSSION AND CONCLUSION

Analysis of hourly tail proton spectra during several months of the deep solar minimum in 2009 reveals the following key findings: (1) Suprathermal proton tails at 1 AU are observed during every hour (except for data gaps) of the quiet 82 days studied. Hourly values of the tail densities range from $5.2 \cdot 10^{-7}$ to $7.3 \cdot 10^{-3}$ cm^{-3} and vary quasi-randomly by factors of ~2 to 10 over periods of one to several hours as well as quasi-periodically by ~20 to 50 over roughly a week. (2) Most (~95%) of the hourly spectra are not power laws, not exponential and not Maxwellians, but multi-component, complex spectra. (3) However, in cases of high tail densities (greater than 10^{-4} cm^{-3}) the tail spectra take on the common (F&G) shapes (-5 power laws with exponential rollovers at some higher speed). Each of the six acceleration events (Figs. 1b and 2) is associated with solar wind compression regions. It is in these local solar wind compression regions where acceleration of particles clearly takes place, and the acceleration process consistently produces F&G spectral shapes. (4) On the other hand, none of the 8 shocks recorded locally outside the local compression regions increased the hourly tail densities significantly nor left any consistent signatures on γ. Finally, the spectrum averaged over the entire 82-day period (Fig. 1a) clearly reveals the existence of the halo solar wind, interstellar pickup protons (seldom seen at 1 AU) and the common F&G tail. It is not surprising to find the common tail shape in this long-term averaged spectrum since the five hourly spectra from the acceleration events contribute most to this 82-day average.

The complex spectral shapes of tails, especially those with the lowest tail densities are most revealing. These spectra (Figs. 3b and 4c) are the superposition of a locally accelerated spectrum starting at the cutoff of the interstellar proton distribution, and a modulated spectrum of protons accelerated at a remote acceleration site in the heliosphere beyond 1 AU. When observed locally, the spectra of particles accelerated remotely (most likely in strong compression regions between CIR shocks) will be modulated due to various transport processes that will progressively suppress the intensity of particles at progressively lower energies (i.e. the modulated spectra will bend downward at low speeds). *Voyager 1* and *2* observed such spectra upstream of the termination shock [2-4,14]. This is what is measured in the heliosheath, where the locally accelerated Termination Shock Particles (TSPs) that have F&G shapes, and the modulated higher energy ACRs combine to form a complex spectrum [3,15].

The following picture then emerges: even during quiet times with few shocks present, the heliosphere still contains some local compression regions that are effective in accelerating suprathermal particles. In these local compression regions the observed spectra have unmistakable F&G shapes, being -5 power laws with an exponential rollover at e-folding speed of (1.4-1.8)•10^8 cm/s. However, at lower tail densities, outside the local compression regions, where most of the hourly spectra are observed, the spectral shapes are complex, a combination of pickup protons at the lowest energy of SWICS and modulated spectra of remotely accelerated particles dominating the higher energy range of SWICS and that of ULEIS. As the tail densities increase the spectra assume more and more the local F&G shape. The fact that the common spectral shape is observed consistently in the local compression regions, and also at all other times even when other spectral features become visible at the lowest and highest energies, provides strong support for the Fisk and Gloeckler pumping mechanism [16-23] for producing suprathermal tails. These tails, created in the quiet solar wind, are most likely the seed spectra for further acceleration by shocks in the heliosphere, in the turbulent solar wind downstream of these shocks, by the termination shock and in the heliosheath.

ACKNOWLEDGMENTS

This work was supported in part by NASA Grant 44A-1085637 (ACE) and by NSF Grant AGS-1043012. We thank E. Möbius and especially P. Bochsler for discussions of analysis of low count data. This paper benefited substantially from discussions held at the meetings of the International Team on -5 Tails and ACRs of the International Space Science Institute in Bern, Switzerland.

REFERENCES

1. G. Gloeckler and L. A. Fisk, "Proton Velocity Distributions in the Inner Heliosheath Derived from Energetic Hydrogen Atoms Measured with Cassini and IBEX" in *Pickup Ions Throughout the Heliosphere and Beyond*, AIP Conference Proceedings 1302, American Institute of Physics, Melville, NY, 2010, pp. 110-116.
2. R. B. Decker, S. M. Krimigis, E. C. Roelof and M. E. Hill, "Particle Acceleration at the Termination Shock: Voyager 1 and 2 Observations" in *Particle Acceleration and Transport in the Heliosheath and Beyond*, AIP Conference Proceedings 1039, American Institute of Physics, Melville, NY, 2008, pp. 349–354.
3. G. Gloeckler, L. A. Fisk, G. M. Mason and M. E. Hill, "Formation of power law tail with spectral index -5 inside and beyond the heliosphere" in *Particle Acceleration and Transport in the Heliosheath and Beyond*, AIP Conference Proceedings 1039, American Institute of Physics, Melville, NY, 2008, pp. 367–374.
4. R. B. Decker, S. M. Krimigis, E. C. Roelof and M. E. Hill, "Foreshock, Termination Shock, and Heliosheath: Voyager 1/2 Observations of Structure and Turbulence" in *Turbulence and Nonlinear Processes in Astrophysical Plasmas*, AIP Conference Proceedings 932, American Institute of Physics, Melville, NY, 2007, pp. 197–202.
5. R. B. Decker, E. C. Roelof, S. M Krimigis and M.E. Hill, "Low-energy Ions Near the Termination Shock" in *Physics of the Inner Heliosheath*, AIP Conference Proceedings 858, American Institute of Physics, Melville, NY, 2006, pp. 73-78.
6. G. Gloeckler and L. A. Fisk, "Acceleration of Low-energy Ions in the Quiet-time Solar Wind and at the Termination Shock" in *Physics of the Inner Heliosheath*, AIP Conference Proceedings 858, American Institute of Physics, Melville, NY, 2006, pp. 153–158.
7. An alternate approach is described by Roelof (this volume).

8. G. Gloeckler et al., *Space Sci. Rev.*, **86**, 495-537 (1998).
9. G. Gloeckler, J. Geiss and L. A. Fisk, "Heliospheric and interstellar phenomena revealed from observations of pickup ions", in *The Heliosphere near Solar Minimum: the Ulysses Perspective*. edited by A. Balogh, E. J. Smith and R. G. Marsden, , Berlin: Springer-Praxis, 2001pp. 287-326.
10. G. M. Mason et al., *Space Sci. Rev.*, **86**, 409-448 (1998).
11. SWEPAM/SWICS Level 3 Solar Wind Proton Data, http://www.srl.caltech.edu/ACE/ASC/.
12. ACE Real-Time Shock solutions, http://www.srl.caltech.edu/ACE/ASC/.
13. N. A. Schwadron, M. A. Dayeh, M. Desai, H. Fahr, J. R. Jokipii, and M. A. Lee, *Astrophysics J.* **713**, 1386 (2010).
14. G. Gloeckler and L. A. Fisk, *Astrophysics J.* **648**, L63-L66 (2006).
15. A. C. Cummings, E. C. Stone, F. B. McDonald, B. C. Heikkila. N. Lal and W. R. Webber, "Anomalous Cosmic Rays in the Heliosheath" in *Particle Acceleration and Transport in the Heliosheath and Beyond*, AIP Conference Proceedings 1039, American Institute of Physics, Melville, NY, 2008, pp. 343–348.
16. L. A. Fisk and G. Gloeckler, *Astrophysics J.* **640**, L79-L82 (2006).
17. L. A. Fisk and G. Gloeckler, *Proc. Nat. Acad. Sci.* **104**, 5749-5754 (2007).
18. L. A. Fisk and G. Gloeckler, *Astrophysics J.* **686**, 1466-1473 (2008).
19. L. A. Fisk, G. Gloeckler and N. A. Schwadron, *Astrophysics J.* **720**, 533-540 (2010).
20. L. A. Fisk and G. Gloeckler, *Advs. Space Res.* **43**, 1471-1478 (2009).
21. L. A. Fisk and G. Gloeckler, *Astrophysics J*, submitted (2011).
22. L. A. Fisk and G. Gloeckler, *Space Sci. Rev.*, submitted (2011).
23. L. A. Fisk and G. Gloeckler (this volume).